JCTC Journal of Chemical Theory and Computation

Article

pubs.acs.org/JCTC

Exploring the Conformational Dynamics of Alanine Dipeptide in Solution Subjected to an External Electric Field: A Nonequilibrium Molecular Dynamics Simulation

Han Wang,*[,†] Christof Schütte,[†,‡] Giovanni Ciccotti,[§,∥] and Luigi Delle Site[†]

[†]Institute for Mathematics, Freie Universität Berlin, 14195 Berlin, Germany

[‡]Zuse Institute Berlin, 14195 Berlin, Germany

[§]School of Physics, University College Dublin, Belfield, Dublin 4, Ireland

[∥]Dipartimento di Fisica, Università "La Sapienza" and CNISM, Piazzale Aldo Moro 5, 00185 Roma, Italy

ABSTRACT: In this paper, we investigate the conformational dynamics of alanine dipeptide under an external electric field by nonequilibrium molecular dynamics simulation. We consider the case of a constant and of an oscillatory field. In this context, we propose a procedure to implement the temperature control, which removes the irrelevant thermal effects of the field. For the constant field different time-scales are identified in the conformational, dipole moment, and orientational dynamics. Moreover, we prove that the solvent structure only marginally changes when the external field is switched on. In the case of oscillatory field, the conformational changes are shown to be as strong as in the previous case, and nontrivial nonequilibrium circular paths in the conformation space are revealed by calculating the integrated net probability fluxes.

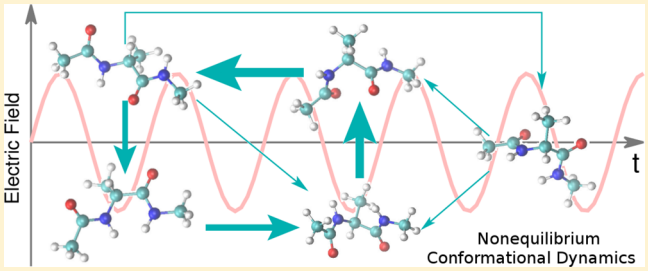

1. INTRODUCTION

The possible effect of the electric field (EF) on the conformation of proteins is a subject of increasing attention because it is linked to the problem of exposing human tissues to electromagnetic radiation. Despite its major relevance, a satisfactory understanding of how the EF influences the behavior of proteins has not been reached so far although a considerable number of experimental[1−5] and theoretical[6−15] studies have been devoted to this topic. In this perspective, molecular dynamics (MD) has been proven useful in understanding the behavior of a protein in both static and oscillatory EF.[6−15] In these studies, the initial configurations are usually taken from the Protein Data Bank (PDB), and then, temperature controlled simulations are performed for a maximum time range of the order of 10−60 ns. During these simulations, time relevant conformational changes characterizing the solvated molecule can be observed. Along the trajectories, various observable, such as the secondary structure, root-mean-square displacement (RMSD), dipole moment, and shape parameters are calculated as a function of time, or in stationary condition, taking time averages. This approach releases useful information on how the secondary structure of the molecule is changed by external EF. However, the behavior of observables in time is characterized by strong fluctuations. The entity of the fluctuations is such that a quantitative analysis becomes difficult and does not allow for a clear understanding of the rationale behind the conformational changes. A time average can reduce the statistical uncertainty; however, in nonstationary conditions this would be a not-well-founded procedure. In fact, we are studying nonstationary nonequilibrium process (e.g., relaxing process to the new conformations under a static EF, or the dynamics from one conformation to the other under an oscillatory EF). In this perspective, if one wants to use MD, the proper way to do it would be that of treating a situation of nonequilibrium with algorithms that can explicitly describe it. This is the approach that will be followed in this work, using the dynamical nonequilibrium molecular dynamics simulation (D-NEMD). The method, first developed by one of us and co-workers,[16−19] has been recently applied to the study of hydrodynamics.[20,21] The essential feature of D-NEMD is to provide a way of evaluating time-dependent nonequilibrium averages starting from a properly determined initial ensemble. In this context, the method can be used to analyze the conformational changes of a solvated molecule, subject to a time-dependent EF.

In the present paper, we study a small peptide, alanine dipeptide, as a model for showing how the method can be used. The choice of a small peptide, rather than a larger one, is done first because it is easier to draw clear conclusions on the nonequilibrium properties of a single peptide by excluding the slow-going interplay between different peptide segments along a chain. Second, the computational cost required is rather massive, and thus, testing the various methodology proposed

Received: November 19, 2013
Published: March 12, 2014

   dx.doi.org/10.1021/ct400993e | J. Chem. Theory Comput. 2014, 10, 1376−1386

here would be hampered for large molecules, although they remain our goal. In any case, alanine dipeptide is large enough so that the conformational changes of its internal degrees of freedom represent valid observables for a test of validity and utility of our approach. The paper is organized as follows: We first describe the idea of D-NEMD and propose a technical improvement consisting in the definition and application of a local thermostatting process. Next, after introducing the physical observables chosen to analyze the nonequilibrium response, the numerical results for the case of a static and oscillatory EF, respectively, are discussed. By calculating the nonequilibrium properties from D-NEMD simulations, we are able to address a few relevant questions: (i) How does the conformation of the peptide changes in an EF (conformational space)? (ii) When do these changes happen (time scale), and how likely are they (probability)? One may wonder whether the information extracted from the D-NEMD simulation could have been extracted just as well from conventional equilibrium simulations. In the Appendix, we show that in this case the D-NEMD approach shall be preferred to the equilibrium approach. The argument is provided by the comparison between the results of the nonequilibrium method and those from equilibrium simulations, within the linear response theory, based on the analysis of correlation functions. To our knowledge, this study is one of the few (if not the first) where time-dependent nonequilibrium with respect to conformation is explicitly considered for a (relatively large) molecule in solution subject to an external time-dependent EF.

2. METHODOLOGY

2.1. Dynamical Nonequilibrium Molecular Dynamics Simulation (D-NEMD). In this section, we briefly review the dynamical approach to nonequilibrium molecular dynamics (D-NEMD).[16,17,20,21] In the following, we denote the macroscopic observable by $O(t)$. If at t the configurational probability distribution is $\rho(\boldsymbol{x},t)$, where $\boldsymbol{x}$ is the phase space variable, then the observable can be expressed by

$$O(t) = \int \mathrm{d}\mathbf{x}\hat{O}(\mathbf{x})\rho(\mathbf{x}, t) = \langle \hat{O}(\mathbf{x}), \rho(\mathbf{x}, t)\rangle \tag{1}$$

We refer to $\hat{O}(\boldsymbol{x})$ as the microscopic observable, which is measured at each point in the phase space $\boldsymbol{x}$. Here we always assume that the initial probability distribution $\rho(\boldsymbol{x},0)$ is known. In particular, in our case, it is identical to the equilibrium distribution of the system without EF. The bracket on the right-hand side of eq 1 denotes, as usual, the inner product in the phase space. We assume that the dynamics of the system is governed by the Hamiltonian equation, that is, $\dot{\mathbf{x}} = J\cdot\nabla_{\mathbf{x}}\mathcal{H}(x, t)$, where $\mathcal{H}$ is the time-dependent Hamiltonian, and J is the symplectic matrix

$$J = \begin{pmatrix} 0 & I \\ -I & 0 \end{pmatrix} \tag{2}$$

The Liouville equation for the probability distribution writes:

$$\frac{\partial\rho(\mathbf{x}, t)}{\partial t} = -iL(t)\rho(\mathbf{x}, t) \tag{3}$$

where $iL(t) = \{\cdot, \mathcal{H}\}$ is the Liouville operator. Equation 3 can be formally solved by $\rho(\boldsymbol{x}, t) = U^{\dagger}(t, 0)\rho(\boldsymbol{x}, 0)$, where $U^{\dagger}(t, 0) = \mathcal{T}\exp\{-i\int_0^t \mathrm{d}t' L(t')\}$, and $\mathcal{T}$ is the time ordering operator. On the other hand,

$$\frac{\mathrm{d}\hat{O}(\mathbf{x}(t))}{\mathrm{d}t} = \nabla_{\mathbf{x}}\hat{O}\cdot\dot{\mathbf{x}} = \nabla_{\mathbf{x}}\hat{O}\cdot J\cdot\nabla_{\mathbf{x}}\mathcal{H} = iL(t)\hat{O}(\mathbf{x}(t)) \tag{4}$$

This equation can be formally solved by $\hat{O}(\boldsymbol{x}(t)) = U(t, 0)\hat{O}(\boldsymbol{x}(0))$, therefore,

$$\begin{aligned} O(t) &= \langle \hat{O}(\mathbf{x}), \rho(\mathbf{x}, t)\rangle = \langle \hat{O}(\mathbf{x}), U^{\dagger}(t, 0)\rho(\mathbf{x}, 0)\rangle \\ &= \langle U(t, 0)\hat{O}(\mathbf{x}), \rho(\mathbf{x}, 0)\rangle = \langle \hat{O}(\mathbf{x}(t)), \rho(\mathbf{x}, 0)\rangle \end{aligned} \tag{5}$$

Since we assume that the system starts from the equilibrium distribution (without EF) eq 5 expresses the fact that the observable $O(t)$ calculated in a situation of nonequilibrium is equal to the ensemble average of the microscopic observable computed along trajectories, starting from initial configurations sampled from an initial or, sometimes, an *equilibrium* distribution. In practical terms, we proceed by first running an equilibrium MD simulation to generate a sample of configurations. Next, we employ these configurations as initial configurations, and for each, the full Hamiltonian dynamics is integrated until time t. In this paper, these trajectories are called *branching trajectories*. Finally, the value of the macroscopic observable at time t is calculated by averaging the microscopic observable measured at each time t along each branching trajectory. Stochastic dynamics (e.g., Langevin dynamics) can be handled analogously.

2.2. Control of Temperature in Nonequilibrium MD. For this study, we are interested in nonthermal[22] effects of the EF on the configuration of the solvated alanine dipeptide. For this reason, a proper control of the temperature in a nonequilibrium system becomes an important issue; in fact, it was argued that an accurate control of the internal reaction temperature is essential to perform reproducible experiments.[12] A straightforward (and realistic) implementation of the temperature control consists in embedding the alanine into an infinitely large solvent environment, and the EF is only applied to the neighborhood of the alanine. In this case, any extra heat generated by the EF can be effectively dispersed in the large solvent environment. In this way one can identify the effect of the EF on the conformational space of the solvated molecule, without the artifact that the surrounding solvent cannot release the additional energy of the EF. However, in practice, in most of the cases the computational cost of having large solvent environment is rather massive if not prohibitive. Therefore, it is of interest to substitute the infinitely large solvent environment with a smaller affordable system and at the same time accurately reproduce the nonequilibrium physical properties of interest. In MD, for equilibrium situations, the solution is to couple the system to an external thermostat, under which the desired ensemble (canonical in this case) can be sampled by simulating a finite size system with periodic boundary conditions. However, coupling the system to a thermostat for nonequilibrium situations is a more delicate issue. In fact, since a thermostat is explicitly designed to bring the system into thermal equilibrium, the perturbation produced by the EF would be mostly adsorbed by the thermostat. This means that the physics of the original dynamics in presence of the EF would be lost and the response to the perturbation would be unphysical.

In this section, we propose a procedure to solve the problem: we start observing that the dynamics without thermostat of the alanine, and the water molecules in the closer solvation shells, is crucial to determine the response of the observable of interest under the EF perturbation (in this work, the observable is the

conformational change of alanine). Instead the detailed dynamics of the water molecules far away is not of primary importance: the region beyond the first solvation shells plays mainly the role of a thermodynamic bath. Therefore, instead of simulating an infinitely large system, we simulate our finite size system with periodic boundary condition, and with the following characteristics: (i) The simulating region is divided in two subregions, a spherical region around the alanine dipeptide of radius R_{ex}, centered at the α-carbon. Here the dynamics is not subject to a thermostat. We refer to such subregion as *the dynamical region*. (ii) Beyond R_{ex}, the dynamics of the water molecules is coupled to a Langevin thermostat. This region is called *the thermostatted region*. For technical convenience, we fix the position of the α-carbon in space, so that the alanine is always located at the center of the simulation region (see Figure 1). In these conditions, the dynamics is preserved in the dynamical region (where the properties of interest are observed), while possible artificial effects of the thermostatting process in the outside region are negligible due to the finite correlation range of liquid water. At the same time, the thermostatted region works as a infinitely large environment that effectively absorbs the extra heat produced by the EF. The validity of the above statements will be checked by a series of numerical tests where it is shown that the response of observables in nonequilibrium (i.e., under the effect of the EF) does not depend on the size of the system and on the size of the dynamical subregion, provided that they are reasonably large. The proposed temperature control method has similarities with the stochastic boundary condition proposed by Brooks and Karplus.[23] However, differently from their approach, we do not explicitly consider a boundary region: The system is instead divided into a dynamical region (corresponding to the reaction region of ref 23) and a thermostatted region (corresponding to the stochastic buffer region in ref 23) in a 3-D cubic periodic simulation box.

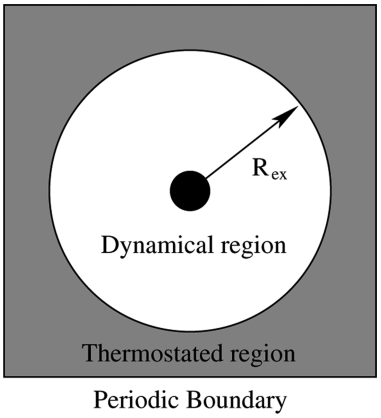

Figure 1. Schematic plot of the nonequilibrium temperature control scheme. The white area is the region characterized by pure dynamics without any direct action by the external thermostat. The gray area is the region where the thermostat is used to keep the target temperature. R_{ex} denotes the size of the purely dynamical region, which is a sphere around the molecule of interest (in our case it is the alanine dipeptide). The whole system is subject to periodic boundary conditions.

3. CASE I: ALANINE DIPEPTIDE UNDER A UNIFORM CONSTANT EF

3.1. System Settings and Simulation Protocol. The system is set up in a 2.7 × 2.7 × 2.7 nm^3 periodic simulation region, with one alanine dipeptide described by the CHARMM27 force field,[24] and dissolved in 644 TIP3P[25] water molecules. The grid-based energy correction map (CMAP)[26] for the backbone dihedral angles is also used. The size of the dynamical region is R_{ex} = 1.0 nm. All simulations are performed by a home-modified GROMACS 4.5[27] together with the CHARMM force field.[28] First, an equilibrium NVT simulation at 300 K of 1000 ns was performed with a Langevin thermostat (time-scale τ_T = 0.5 ps). Along the trajectory, configurations were taken every 0.5 ns and we used 2000 initial configurations for each nonequilibrium MD simulation (if not stated otherwise for specific cases). The branching trajectories were integrated by the Leap-frog scheme (standard Gromacs implementation) with the aforementioned nonequilibrium temperature control technique. The time step was 0.002 ps. The short-range interaction (van der Waals interaction) had a cutoff radius of 1.0 nm and had been smoothed from 0.8 to 1.0 nm by the "switch" method provided by the GROMACS code. A energy conserving Particle Mesh Ewald (PME)[29,30] method was applied to calculate the electrostatic interaction in this periodic system. For the direct space part of PME the cutoff and smoothing follow the same principles as those applied to the van der Waals interaction. All hydrogen involving bonds were constrained by LINCS,[31] except the TIP3P water

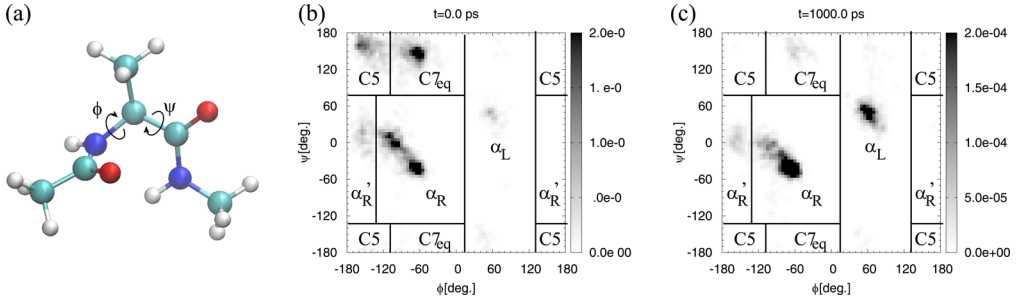

Figure 2. Probability density of the conformations of the alanine dipeptide plotted on the Ramachandran plot. (a) Two dihedral angles ϕ and ψ are used to represent the molecular conformations of the alanine dipeptide. (b) The equilibrium probability density at t = 0 ps. (c) The probability density of equilibrium at t = 1000 ps, resulting from the application of a constant EF of 1 V/nm. Darker color indicates higher probability. Plots are divided into 5 subregions corresponding to 5 molecular conformations: $\alpha_R = \{(\phi, \psi) | -134° \le \phi < 13°, -125° \le \psi < 74°\}$, $\alpha'_R = \{(\phi,\psi) | 128° \le \phi < 226°, -125° \le \psi < 74°\}$, $C7_{eq} = \{(\phi, \psi) | -110° \le \phi < 13°, 74° \le \psi < 235°\}$, C5 = $\{(\phi, \psi) | 128° \le \phi < 250°, 74° \le \psi < 235°\}$, $\alpha_L = \{(\phi, \psi) | 13° \le \phi < 128°, -180° \le \psi < 180°\}$. Considering the angular periodicity, the angle, for example, 226° corresponds to −134° on plots b and c. This division is the same for both plots b and c.

dx.doi.org/10.1021/ct400993e | J. Chem. Theory Comput. 2014, 10, 1376−1386

molecules, which were constrained by the SETTLE algorithm.[32] In the thermostatted region, the original dynamics was coupled to a Langevin thermostat with $\tau_T = 0.1$ ps. In all testing cases, this local thermostat is able to control the system at the desired temperature, that is, 300 K (the results are not presented in this paper). The whole system is also coupled to a Parrinello−Rahman barostat[33] (in standard Gromacs implementation) with $\tau_P = 2.0$ ps to keep the pressure at ambient condition (1 bar). Since the change of the system size is small and slow, the pressure control does not have an sizable effect on the dynamics of the system. At time $t = 0$ ps, the system has been fully equilibrated without any EF. From $t = 0$ to the warm-up time $t = t_{warm}$, the EF is switched on linearly, while after $t = t_{warm}$, the field is kept constant in time at E_∞. In this work, we consider $t_{warm} = 10$ ps and $E_\infty = 1$ V/nm. The direction of the field is arbitrarily chosen along the x direction. In this paper, we denote the EF as a function of time $\boldsymbol{E}(t)$. Therefore, for the case of constant EF, we have $\boldsymbol{E}(t) = (E_\infty \cdot t/t_{warm}, 0, 0)$ for $0 \le t < t_{warm}$, and $\boldsymbol{E}(t) = (E_\infty, 0, 0)$ for $t \ge t_{warm}$.

3.2. Molecular Conformation and Net Probability Flux. The change of conformation in time of the alanine dipeptide is investigated by analyzing the probability density $p(\phi, \psi, t)$ on the Ramachandran plot at time t. The definition of the dihedral angles ϕ and ψ is given in Figure 2a. The probability density of conformations of equilibrium in absence of external field is shown in Figure 2b, while the same quantity, resulting from the molecular relaxation to the action of $E_\infty = 1$ V/nm is given in Figure 2c. In the plot one can identify several clusters in which conformations are grouped. Therefore, in order to simplify the analysis, we divide the Ramachandran plot into 5 subregions $\{\alpha_R, \alpha'_R, C7_{eq}, C5, \alpha_L\}$ (see caption of Figure 2 for the corresponding definition). It is worth to notice that these conformations are found in different secondary structures of a peptide chain: α_R and α'_R correspond to the α-helix. $C7_{eq}$ and C5 correspond to the β-sheet. α_L corresponds to the left-handed α-helix.

From Figure 2, it is evident that the probability with which a conformation occurs changes when the external EF is applied. The most evident case is conformation α_L; in fact, it is almost not present before the external field is applied but appears in a clear way as a response to the action of the EF. Following this line of thought, we are interested to study the change of conformation under the action of EF. Specifically, for each conformational change, we will analyze the relation between the structural relaxation of the molecule and its corresponding time scale. The starting point is the calculation of the probability of each conformation:

$$P_I(t) = \mathbb{P}((\phi_t, \psi_t) \in I),$$
$$I \text{ being one of the five regions} \{\alpha_R, \alpha'_R, C7_{eq}, C5, \alpha_L\} \tag{6}$$

Notice that the probability is time dependent, being an observable in nonequilibrium situation. Next, we consider the *net probability flux* from conformation J to I, defined by

$$F_{J,I}(t) = \frac{1}{\Delta t}[\mathbb{P}((\phi_{t-\Delta t}, \psi_{t-\Delta t}) \in J, (\phi_t, \psi_t) \in I) - \mathbb{P}((\phi_{t-\Delta t}, \psi_{t-\Delta t}) \in I, (\phi_t, \psi_t) \in J)],$$
$$J, I \in \{\alpha_R, \alpha'_R, C7_{eq}, C5, \alpha_L\} \tag{7}$$

where $\mathbb{P}((\phi_{t-\Delta t}, \psi_{t-\Delta t}) \in J, (\phi_t, \psi_t) \in I)$ is the joint probability of the alanine being in conformation J at time $(t - \Delta t)$ *and* being in conformation I at time t. The same definition applies to $\mathbb{P}((\phi_{t-\Delta t}, \psi_{t-\Delta t}) \in I, (\phi_t, \psi_t) \in J)$. Here, the time interval Δt should be small enough compared to the time scale of conformational dynamics, so that the changes in the conformation probabilities can be treated in linear approximation. At the same time, Δt should be also large enough compared with the time step of the MD integrator, so that the quantities of eq 7 are well-defined and can be estimated with sufficient numerical accuracy (see also ref 34). In all the numerical examples of this work, $\Delta t = 1$ ps is used. A positive value of $F_{J,I}(t)$ indicates that the net flux goes from J to I, while a negative value indicates a net flux from I to J. Through $F_{J,I}(t)$, the analysis of the nonequilibrium process is projected onto the analysis of the probabilistic link between discretized conformations $\{\alpha_R, \alpha'_R, C7_{eq}, C5, \alpha_L\}$. The concept of net probability flux employed by us is very close to the concept of kinetic rate. However, we prefer to stick to our definition which is mathematically simpler and univocal. In the case of oscillatory EF, the behavior of the net probability flux is also highly oscillatory, thus, in order to clearly identify the essential features of the molecular conformational changes, it is convenient to study the integrated net probability flux, defined as

$$Q_{J,I}(t) = \int_0^t F_{J,I}(\tau)\mathrm{d}\tau \tag{8}$$

which expresses the cumulative effects due to the action of EF on the conformations of the molecule.

3.3. Conformational Dynamics. The time-dependent probability density of the system to stay in a certain conformation is given in Figure 3. In order to show that our simulation results are robust with respect to the randomness introduced by the (local) Langevin thermostat, we have tested the effects of changing random seeds for the thermostat in the

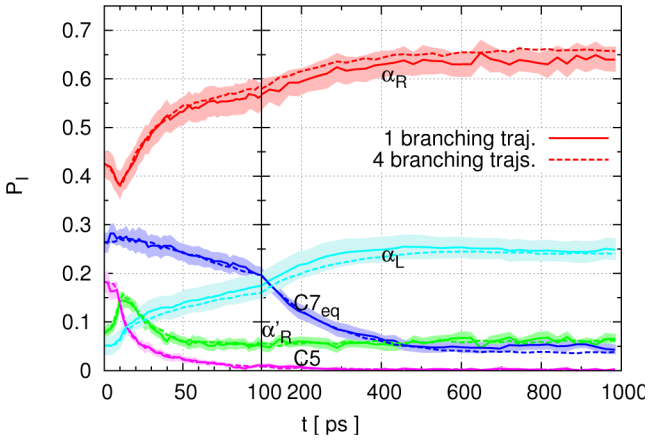

Figure 3. Time-dependent probability of conformations $P_I(t)$ when a constant EF is present, where $\sum_I P_I(t) = 1$, $\forall t$. The warm-up time is $t_{warm} = 10$ ps. The red line refers to conformation $I = \alpha_R$, green to α'_R, dark blue to $C7_{eq}$, purple to C5 and light blue to α_L. The solid lines denote the results of one branching trajectory starting from each initial conformation, while the dashed lines denote the average of the four branching trajectories (different random seeds for the Langevin thermostat, see text) starting from each initial conformation. The shadowed region with each solid line denotes the statistical uncertainty of the result at 95% confidence level.

dx.doi.org/10.1021/ct400993e | J. Chem. Theory Comput. 2014, 10, 1376−1386

thermostatted region. We compared simulation results obtained by starting a branching trajectory from each initial conformation with those obtained from four different branching trajectories from each initial conformation (each of four with different random seed for the Langevin thermostat in the thermostatted region). Results are consistent within the statistical uncertainty (see Figure.3). The β-sheet conformations $C7_{eq}$ and C5, which are present at the initial stage after EF is switched on, fade away as the system relaxes. The probability of the α-helix conformation α_R, grows from 0.43 to 0.65. The α-helix α'_R does not change significantly under the action of EF. The left-hand helix conformation α_L noticeably grows from 0.05 to 0.25. We plot the net probability fluxes of the four-branching-trajectories case in Figure 4. Results show that for

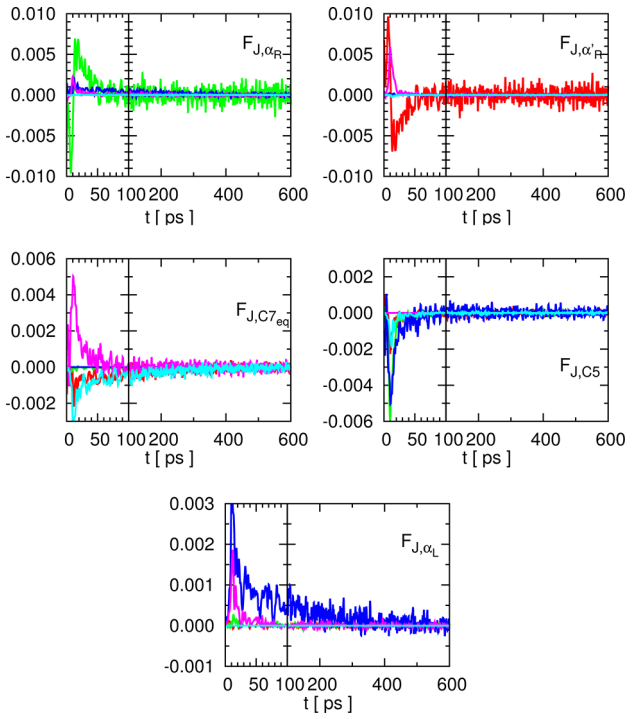

Figure 4. Net probability flux for the constant EF case. The warm-up time is t_{warm} = 10 ps. The probability flux $F_{J,I}(t)$ (defined by eq 7) is reported in units of ps^{-1}. From top to bottom, left to right, we report $I = \alpha_R$, α'_R, $C7_{eq}$, C5 and α_L, respectively. In each plot, the red line stands for $J = \alpha_R$, green for $J = \alpha'_R$, dark blue for $J = C7_{eq}$, purple for J = C5, and light blue for $J = \alpha_L$. This plot is drawn from the four-branching-trajectories case (see the text).

short t, the net fluxes are generally nonzero; however, as t goes to infinity, all fluxes converge to zero. This indicates that, as the EF is switched on, the system is driven away from the initial equilibrium (at zero EF), starting a dynamical nonequilibrium process. After sufficiently long time, the system is fully relaxed to the new stationary state, in which it remains as long as the EF is switched on. Of course, we cannot exclude very slow nonequilibrium processes, which cannot be captured by the duration of our nonequilibrium simulation (1 ns), since it is obviously that the proposed nonequilibrium approach can only study time-dependent behaviors that are shorter than the total time of the branching trajectories. An important point is that despite the system is finally relaxed to the new conformation, the relaxation time scales corresponding to each conformation are rather different. From Figure 3 and 4, we observe mainly three different time scales 10, 100, and 500 ps, whose corresponding conformations are summarized in Table 1.

Table 1. List of the Main Probability Fluxes and the Corresponding Time Scales Observed in the Constant EF Case

direction	time scale [ps]
$\alpha_R \rightarrow \alpha'_R$	~10
$C5 \rightarrow \alpha_R,\alpha'_R,\alpha_L$	~50
$\alpha'_R \rightarrow \alpha_R$	~100
$C5 \rightarrow C7_{eq}$	~100
$C7_{eq} \rightarrow \alpha_R,\alpha_L$	~500

This is a relevant result because it shows the possibility of employing an external EF as a tool to identify relevant time scales in the conformational behavior of a molecule in solution.

3.4. Molecular Dipole Response. The fact that our external perturbation corresponds to the action of an electric field, naturally leads to the question of the alignment of the molecular dipole vector along the direction of external EF, and, in turn, of how this is related to the overall conformational change of the molecule as reported in the previous section.

The dipole moment of the alanine dipeptide is defined by

$$\boldsymbol{\mu}_{\text{alanine}}(t) = \left\langle \sum_{i \in \{\text{point charges of alanine}\}} q_i \mathbf{r}_i(t) \right\rangle \quad (9)$$

where q_i denotes the partial charge of any point charge i defining our model of alanine, the molecule being neutral, that is, $\Sigma_i q_i = 0$. $\mathbf{r}_i$ denotes the position of the point i. Figure 5 shows

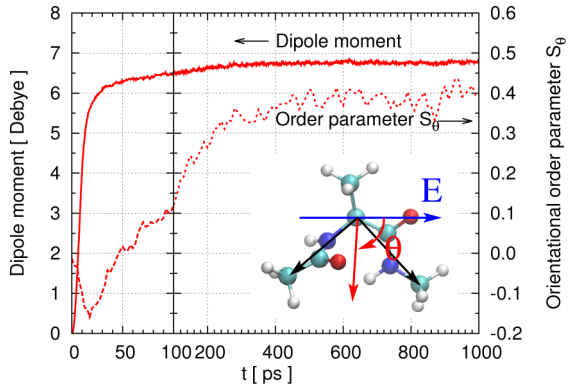

Figure 5. x-Component of the molecular dipole moment and the orientational order parameter of the alanine molecule as a function of time. The solid line represents the dipole moment, while the dashed line represents the orientational order parameter. The left vertical axis is for the dipole moment, while the right is for the orientational order parameter.

that the x-component of the dipole moment reaches 85% of its maximum value in only 20 ps, which is comparable to the warm-up time t_{warm} and is 25 times smaller than the slowest time scale of the conformational relaxation. Then, in the following 400 ps, the dipole slowly relaxes to its maximum value, that is, 6.8 D, and corresponds to an energy ($\boldsymbol{\mu}_{\text{alanine}} \cdot \boldsymbol{E}$) of c.a. −13.6 kJ/mol. We calculated the averaged dipole moment of different conformations (defined by taking averages in eq 9 only for given conformations) under constant EF, and found 6.8, 6.0, 5.1, 3.1, and 7.1 D for α_R, α'_R, $C7_{eq}$, C5, and α_L, respectively. The dipole energy difference between 3.1 and 7.1 D is roughly 8.0 kJ/mol. Under a constant EF, the system will

dx.doi.org/10.1021/ct400993e | J. Chem. Theory Comput. 2014, 10, 1376−1386

be likely to be driven toward those conformations with higher dipole moment, because the energy of the system will be lowered. We suggest that this energy difference may be the reason why we observe that the β-sheet conformations with lower dipole moment are driven toward α-helix conformations α_R and α_L, whose dipole moments are the highest among all conformations. Moreover, the C5 conformation vanishes because its dipole is significantly lower than other conformations. Comparing Figure 5 with 3, the sharp increment of dipole moment before 20 ps is due to the quick vanishing of conformation C5, while the slow increment of dipole moment until 400 ps is due to the slow migration from conformation $C7_{eq}$ to α_R and α_L.

3.5. Response of the Orientational Order Parameter. As a complementary information to the behavior of the molecular dipole moment it is of interest to describe the overall orientational behavior of the molecules with respect to the EF. In fact, while the dipole moment specifically expresses the rearrangement of charges within the molecule as a response to the EF, the overall direction of the molecule tells us about the interplay between the internal positional rearrangement of the atoms and their alignment with respect to the EF. To this aim, let us define the geometric direction of the alanine by the red vector in the inset in Figure 5, that is, by the angle bisector of the two black vectors, which connect the α-carbon and the carbons on the methyl groups. We considered the angle θ made by the orientation of the alanine dipeptide in space with respect to the direction of EF as a function of time. Then, we defined an orientational order parameter

$$S_\theta = \langle 3\sin^2\theta - 2\rangle \tag{10}$$

The ensemble average is made along the branching trajectories, so it is a time dependent observable. The order parameter indicates the (time dependent) average orientation of the molecule with respect to the direction of the EF. If the molecule is perfectly perpendicular to the EF, then $S_\theta = 1$; if it is perfectly parallel, then $S_\theta = -2$; if it has no directional preference, then $S_\theta = 0$. From $t = 0$ to roughly 10 ps, the orientational order parameter rapidly decreases from 0 to −0.15, which means a weak alignment of the molecule to the external field. Then, from $t = 10$ to 500 ps, the molecule slowly changes to the orientation that is almost perpendicular to the EF. In fact, the vector of the geometric direction tends to be perpendicular to the dipole moment, if one observes the correlation between the value of the dipole moment (which tends to be more parallel to the EF as its value increases) and the angle of the vector of the geometric direction, the result above can be easily explained. This orientational change is linked to the observed slowest time scale of the molecular conformational change.

3.6. Effects of EF on the Solvent around the Molecule. So far, we have focused our attention on the behavior of the alanine under the action of the EF. However, it is also important to understand the effects of the EF on the solvating water molecules. Being water a polar molecule the electrostatic interaction with an EF can dramatically change its solvation structure around the alanine and thus, in turn, influence its conformational behavior. For this reason, in this section, we analyze the behavior of the solvent around the alanine under the action of the EF by investigating the radial distribution function (RDF) between α-carbon and the center-of-mass (COM) of the water molecules (see Figure 6a). The average RDF does not change significantly as a function of time (within the statistical error). Figure 6b presents the number of hydrogen bonds between the alanine and water molecules and between two neighboring water molecules. The number of hydrogen bonds are calculated by standard GROMACS routine g_hbond, with donor−acceptor distance cutoff 0.3 nm, and hydrogen-donor−acceptor angle cutoff 20°. We observe that the number of hydrogen bonds remains almost the same when the EF is turned on, although molecular dipoles tend to align along the direction of the EF (result not shown). The EF-induced solvent effect on the alanine can be also accounted by calculating the difference of the water−alanine electrostatic interaction without and with the EF. The energy difference is found to be −19.1 kJ/mo, which is comparable to the electrostatic energy associated to the dipole of the alanine itself. Therefore, we conclude that the solvation structure around the alanine does not change or contribute significantly in determining the conformational dynamics of the alanine under the action of EF.

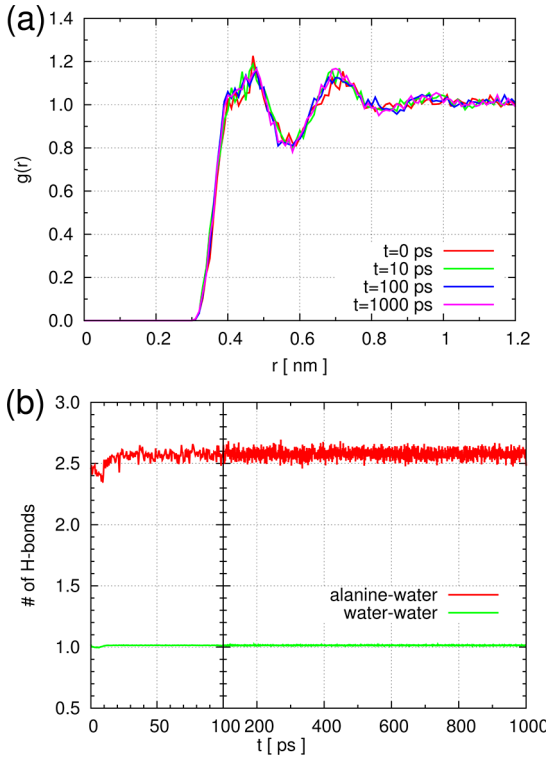

Figure 6. Solvent structure around the alanine dipeptide. (a) The radial distribution function (RDF) between the α-carbon and the center-of-mass (COM) of the water molecules at $t = 0$, 10, 100, and 1000 ps. (b) The number of hydrogen bonds formed between the alanine and water and between two water molecules. The number of hydrogen bonds between two water molecules is normalized by the number of water molecules in the system.

3.7. Finite-Size Effect on the Dynamical and Thermostatted Regions. Just as described in section 2.2, we performed nonequilibrium MD simulations in a finite size periodic system, further divided into a dynamical and a thermostatted region. Since the periodic boundary conditions and the division of the system are technical approximations to the real system with dynamics-preserving thermal control, the effect of the finite-size in the system settings should be carefully checked. Therefore, we perform two additional simulations: one with box dimensions $L = 4.0$ nm (the box is cubic) and a Hamiltonian dynamical region of radius $R_{ex} = 1.0$ nm. A second

dx.doi.org/10.1021/ct400993e | J. Chem. Theory Comput. 2014, 10, 1376−1386

simulation is done with box size L = 4.0 nm and a dynamical region of radius R_{ex} = 1.5 nm. We compare the results of these two simulations to those of the system we have used so far, that is, L = 2.7 nm and R_{ex} = 1.0 nm. Figure 7 shows essential consistency in the simulation results for the three systems. The finite-size effects are negligible.

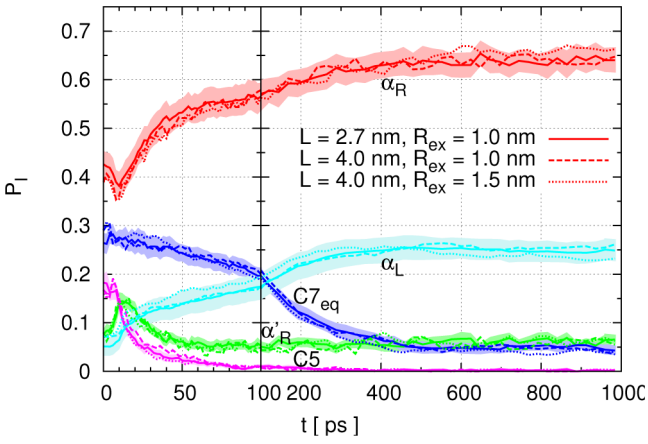

Figure 7. Testing the finite-size effect on the dynamical and thermostatted region. Probabilities of different conformations are presented versus time. See the text for more details. The shadowed region denotes the statistical uncertainty of the L = 2.7 nm, R_{ex} = 1.0 nm case at 95% confidence level.

4. CASE II: PERIODICALLY OSCILLATORY EF

A step forward in our study is to consider a periodically oscillatory EF, which has a sin-wave shape:

$$\mathbf{E}(t) = (E_0 \sin(2\pi t/T_P),\ 0,\ 0) \tag{11}$$

where E_0 is the intensity of the field, which is chosen to be 1.0 V/nm. T_P is the oscillating period. Here, we tested three different periods 10, 40, and 200 ps. Figure 8a presents the x-component of the molecular dipole moment as a function of time. The red, green, and blue lines report the results of T_P = 10, 40, and 200 ps, respectively. The black line shows the dipole moment under constant EF for reference. It shows that the oscillating period of the molecular dipole moment is the same as the period of the oscillatory EF. Therefore, the molecular dipole moment is able to respond to the external EF almost immediately. At T_P = 200 ps, the maximum magnitude of the molecular dipole moment is close to the value obtained in the case of constant EF, which means that the variation of the oscillatory EF is so slow that the alanine has enough time to relax its dipole. However, for T_P = 10 and 40 ps, the EF oscillates faster and the molecule does not have enough time to fully relax the dipole, as a consequence the maximum dipole moment is smaller than the previous case. Figure 8b presents the orientational order parameter. The notations are the same as Figure 8a. For all cases the order parameter is much smaller than in the case of constant EF. One possible reason is that the relaxation of the order parameter is very slow and the molecule in the case of oscillatory field is not exposed to a strong enough EF for a time long enough. For T_P = 10 and 40 ps, the orientation of the alanine shows a very weak tendency to be parallel to the EF. It is worth to notice that for constant EF, we also observe a quick alignment of the molecular orientation vector to the EF on the time scale of 10 ps. For T_P = 200 ps, the

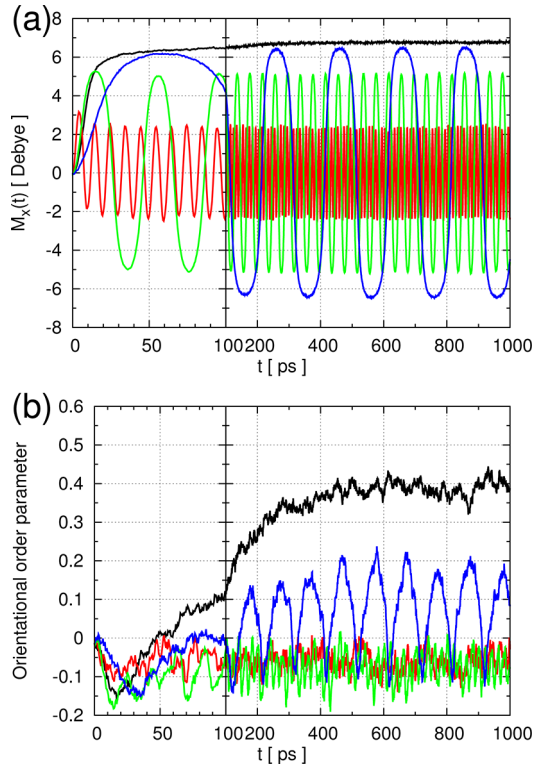

Figure 8. Illustration of the effect of the oscillatory EF on the system: (a) the dipole moment and (b) the orientational order parameter of alanine dipeptide as a function of time. In plot a, only the x-component of the dipole moment is shown. The black line refers to the static EF which is turned on at time t_{warm} = 10 ps. The red line refers to the oscillatory field with period of 10 ps. The green line is of 40 ps and the blue of 200 ps.

molecule tends periodically to be more perpendicular to the EF, but this directional preference is much weaker than in the case of constant EF.

Figure 9 shows the probability of the conformations against time for periodically oscillatory EF, while Figure 10 presents the integrated net probability fluxes (defined by eq 8) between conformations. Here, the probability fluxes are not reported because the profiles are highly oscillating and they would not offer a better information than the one that can be obtained from the integrated probability flux. Coming back to Figure 9, for all periods investigated, the observed time-dependent probabilities in α_R, α'_R, $C7_{eq}$, and C5 are highly oscillating and the average value over time cycles does not change considerably with respect to time. However, the probability in conformation α_L significantly increases to approximately 0.17 for T_P = 10 ps, 0.27 for T_P = 40 ps, and 0.26 for T_P = 200 ps. In the case of T_P = 10 and 40 ps, the probability of conformation α_L reaches the steady value in around 300 ps, while it requires about 1200 ps for the T_P = 200 ps case. The notable increment of probability of α_R and the vanishing of $C7_{eq}$ in the constant EF case (see Figure 3) are not observed in the oscillatory EF case. In comparison to the static EF case, where the probability flux vanishes when the system reaches steady state (Figure 4), Figure 10 shows increasing integrated probability net fluxes, which imply some lasting and directional fluxes among the conformations in steady state. Figure 11 presents a schematic plot of the main probability fluxes for T_P = 10 ps. The thickness of the arrows and the numbers nearby indicate the steady value of average net fluxes over periods. The relevance of Figure 11 is

dx.doi.org/10.1021/ct400993e | J. Chem. Theory Comput. 2014, 10, 1376−1386

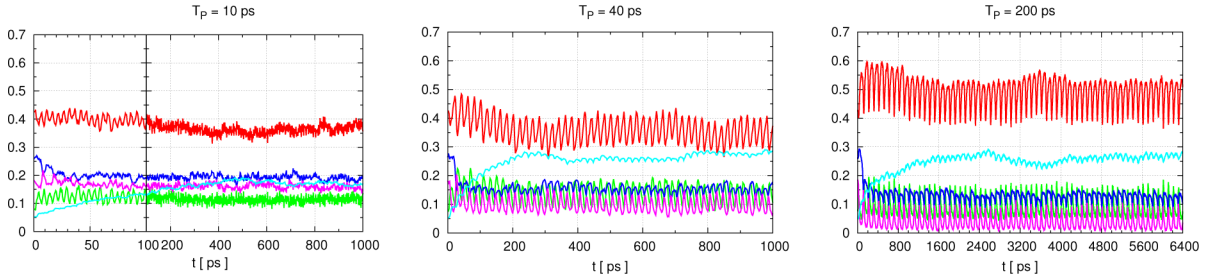

Figure 9. Probability of being in a given of conformation for alanine in a periodically oscillatory EF. Different periods, that is, T_P = 10 , 40, and 200 ps, are considered here. The probability of being in a certain conformation I, which is denoted by P_I in this paper, is plotted by colored lines against time. Red line, $I = \alpha_R$; green line, $I = \alpha'_R$; dark blue line, I = C7$_{eq}$; pink line, I = C5; and light blue line, $I = \alpha_L$. For T_P = 10 and 40 ps, the nonequilibrium simulations last 1000 ps, while for T_P = 200 ps, they last 6400 ps.

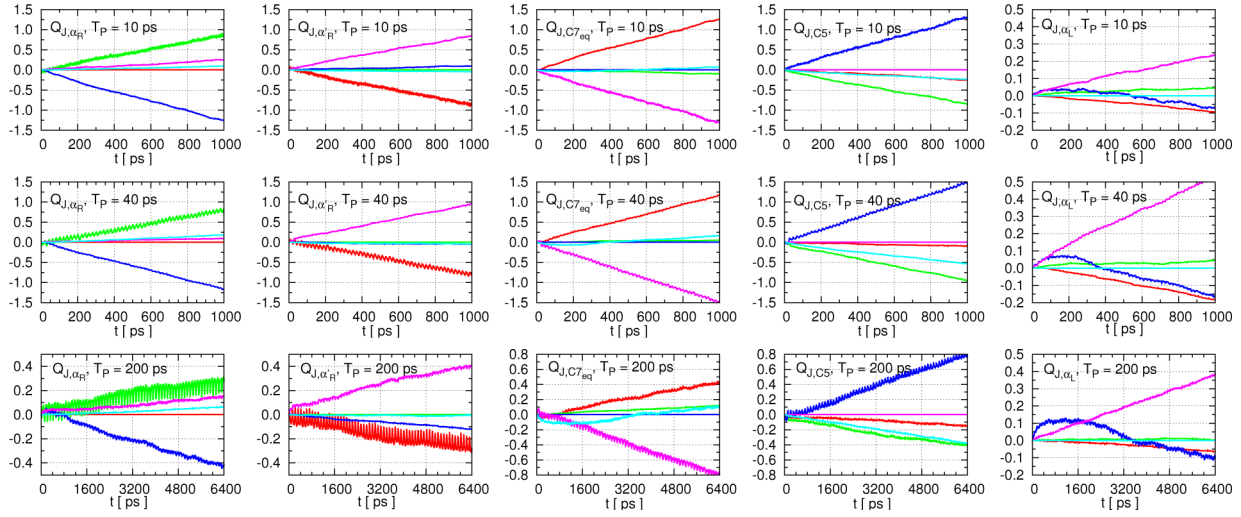

Figure 10. Integrated probability flux $Q_{J,I}(t)$ for the periodically oscillatory EF, is plotted against time (horizontal axis, in picoseconds). The integrated probability flux is defined by $Q_{J,I}(t) = \int_0^t F_{J,I}(\tau)d\tau$, where $F_{J,I}(t)$ is the net probability flux from conformation J to I. See also eq 7 and 8 for definitions of $F_{J,I}(t)$ and $Q_{J,I}(t)$, respectively. From top to bottom, rows report results with period 10, 40, and 200 ps, respectively. From left to right, the five columns show the integrated flux Q_{J,α_R}, Q_{J,α'_R}, $Q_{J,C7_{eq}}$, $Q_{J,C5}$, and Q_{J,α_L}, respectively. In each plot, the red line stands for $J = \alpha_R$, green for $J = \alpha'_R$, dark blue for J = C7$_{eq}$, purple for J = C5, and light blue for $J = \alpha_L$. An increasing value of $Q_{J,I}$ indicates a net probability flux from conformation J to I, while a decreasing value of $Q_{J,I}$ indicates a net probability flux from I to J.

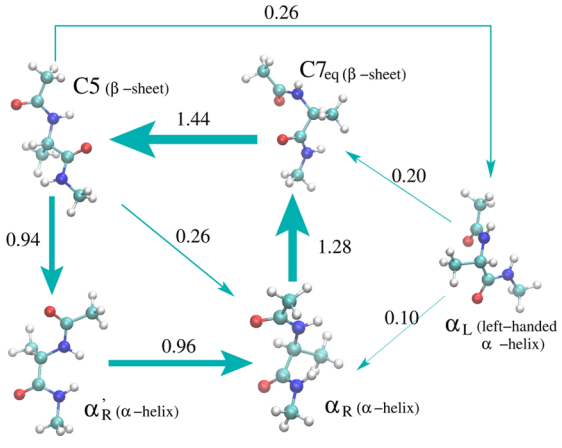

Figure 11. Schematic plot of the main probability fluxes between conformations for oscillatory EF, T_P = 10 ps. The thickness of the arrows approximately presents the strength of the flux. The numbers near the arrows indicates the strength of the averaged probability flux, the unit of which is $10^{-3} \times ps^{-1}$.

in the fact that it suggests, in perspective, a general scenario common to all molecules characterized by β-sheet-like or α-helix-like conformations and how an electric field is likely to modify it. Although the network presented in Figure 11 is similar to those discovered in the equilibrium studies in the sense of the steady conformations and connections among them (e.g., in refs 35 and 36), the physical meaning is quite different in our study: The system is under nonequilibrium conditions due to a controlled physical external perturbation, and the related net probability fluxes are based on trajectories generated by such a perturbation. In contrast, in the equilibrium studies, such net probability fluxes do not explicitly exist. The probability flux of T_P = 40 ps is quantitatively comparable to the case T_P = 10 ps, except that the probability fluxes going into conformation α_L is stronger, which actually results in a higher steady probability in α_L. The probability flux of case T_P = 200 ps is qualitatively similar to T_P = 10 ps and T_P = 40 ps; however, the strength is much lower than the latter two cases. Moreover, we see that the integrated fluxes reach a steadily increasing stage after about 3200 ps, which is even longer than the time scale at which the probability of α_L reaches its steady value. This indicates a longer intrinsic time scale in the T_P = 200 ps case.

We have not studied periods longer than T_P = 200 ps, because the trend suggests that a longer period indicates even

dx.doi.org/10.1021/ct400993e | J. Chem. Theory Comput. 2014, 10, 1376–1386

longer intrinsic time scales. However, the long-period-limit case can be safely guessed: When the EF changes so slowly that at each time the system can be viewed as in equilibrium, the process falls in the category of a quasi-equilibrium process.

5. DISCUSSION AND CONCLUSION

We have investigated the conformational dynamics of a solvated alanine dipeptide under the action of a constant and oscillatory electric field (EF). We have employed the dynamical nonequilibrium molecular dynamics (D-NEMD) method. This allowed us to analyze the conformational changes of the molecule in terms of a response to an external perturbation which drives the system away from equilibrium. From the technical point of view, we have proposed a local thermostatting procedure that does not introduce invalidating artifacts and, at the same time, avoids the necessity of considering large water bulk systems to solvate the molecule. The conformations of the alanine dipeptide are first projected onto the Ramachandran plot and then grouped in five conformations. These conformations correspond to different secondary structures in larger molecules (i.e., proteins). Next, the time-dependent probability of being in a certain conformation and the net probability flux between them are calculated. We have compared the case of constant EF and that of oscillatory EF and reported the main differences. Worthy of notice is the possibility of employing an EF in order to identify several time scales related to conformational changes, this would not be straightforward for standard equilibrium MD simulations and thus suggest that D-NEMD proposed here is a powerful tools to investigate the conformational properties of a large molecule in solution.

The intensity of the EF used in this paper is 1 V/nm for both constant and oscillatory cases. This intensity is 4−5 orders of magnitude higher than that reachable in a standard laboratory microwave instrument.[12] However, this intensity is achievable by a sharp electric field emitter tip,[37] near the surface of mica,[13] or by a modern laser equipment.[38] The minimal frequency investigated here (5.00 GHz, i.e., T_P = 200 ps) is of the same order of magnitude as the microwave radiation available in laboratory (2.45 GHz).[12] The highest frequency (100 GHz, i.e., T_P = 10 ps) is 1 order of magnitude lower than the tetrahertz spectroscopy experiments,[39,40] so our results cannot be directly connected to these experimental results. The authors are fully aware that the EFs investigated in the present paper are, at this stage, still ideal, above all regarding their spatially homogeneity and the fact that the time-dependency is always well-defined (as pointed out by previous simulation studies[6−15]). However, the present work is an attempt to understand how the use of D-NEMD as a simulation tool can be applied to the important case of an EF and which information one may extract that is not easily accessible to other MD procedures (e.g., EF induced conformational changes and its related time scales which opens the possibility of conformational manipulation of the protein by applying an external EF.)

In order to sharply define the advantages and limitations of the approach used, we must also clarify that in order to describe the system we use a classical force field with TIP3P water model. The EF is well know to be able to protonate the water molecule at the intensity we used in the paper. However, this happens at the time scale of femtoseconds, which is much shorter than the slowest time scale resolved by the current research, so on average it should not play an essential role on the conformational dynamics. The polarization with respect to the external EF also does not play a important role, because under the EF of 1 V/nm, the induced dipole of water is only c.a. 0.05 D that is negligible comparing with the dipole moment response observed in our simulations. Therefore, it is reasonable to use a nonpolarizable model in this study. The reason we prefer a rigid water model is that it is computationally more efficient than any polarizable water model. We also want to remind the reader that it has been reported recently that the physical scale of the slowest dynamics differs in a considerable way between different force fields.[41] However, the main qualitative conclusions, for example those concerning the determination of time scales or the map of conformational changes, are not likely to change significantly as a function of the force field.

APPENDIX: COMPARISON WITH THE LINEAR RESPONSE THEORY

A commonly used equilibrium approach that can describe the nonequilibrium response is the linear response theory (Green-Kubo relation[42,43]). We employed such a method to test the conformational dynamics of alanine dipeptide under the EF. The response function, for example, the time-dependent probability of left-handed α-helix, is defined as[44]

$$P_{\alpha_L}(t) = \langle \chi_{\alpha_L}(t) \rangle \approx \langle \chi_{\alpha_L} \rangle_0 - \beta \int_0^t \mathrm{d}s M_e(t-s) \langle j(0) \cdot \chi_{\alpha_L}(t) \rangle_0 \quad (12)$$

where χ_{α_L} is the characteristic function of set α_L that takes the value of 1 for $(\phi, \psi) \in \alpha_L$, and takes value 0 otherwise. $M_e(t)$ is the relative magnitude of the EF. For the case of constant EF, for example, $M_e(t) = t/t_{warm}$ for $0 \le t < t_{warm}$, and $M_e(t) = 1$ for $t \ge t_{warm}$. j is the dissipative flux that is defined by

$$j = -\sum_{i=1}^{N} E_\infty q_i v_{i,x} \quad (13)$$

where q_i is the partial charge of the ith atom, and $v_{i,x}$ is the x component of the velocity of the ith atom. The notation $\langle \cdot \rangle_0$ denotes the equilibrium ensemble average. We report the correlation function $\langle j(0) \cdot \chi_{\alpha_L}(t) \rangle_0$ as a function of correlation time t in Figure 12a. The value of the function is estimated from two independent 1 μs equilibrium simulations. It must be noticed that the total length of the equilibrium trajectories is the same as the nonequilibrium simulation (2000 trajectories, each 1000 ps long). Results show that the statistical error is much larger than the value of correlation function itself. In Figure 12b, the probability of conformation α_L calculated from the linear response theory (12) is compared with that computed from D-NEMD (1). The linear response result follows the D-NEMD result only in the very first 15 ps; then, it diverges. Since it is meaningless for a probability being larger than 1, the linear response result is qualitatively wrong. Therefore, the overwhelming statistical uncertainty suggest to prefer D-NEMD eq 1 to calculate the nonequilibrium averages. In fact, since the total computational effort of the equilibrium simulation is the same as the nonequilibrium simulation, the nonequilibrium simulation is more accurate than the conventional equilibrium approach (linear response) at the same computational cost. A similar observation has already been reported in ref 16.

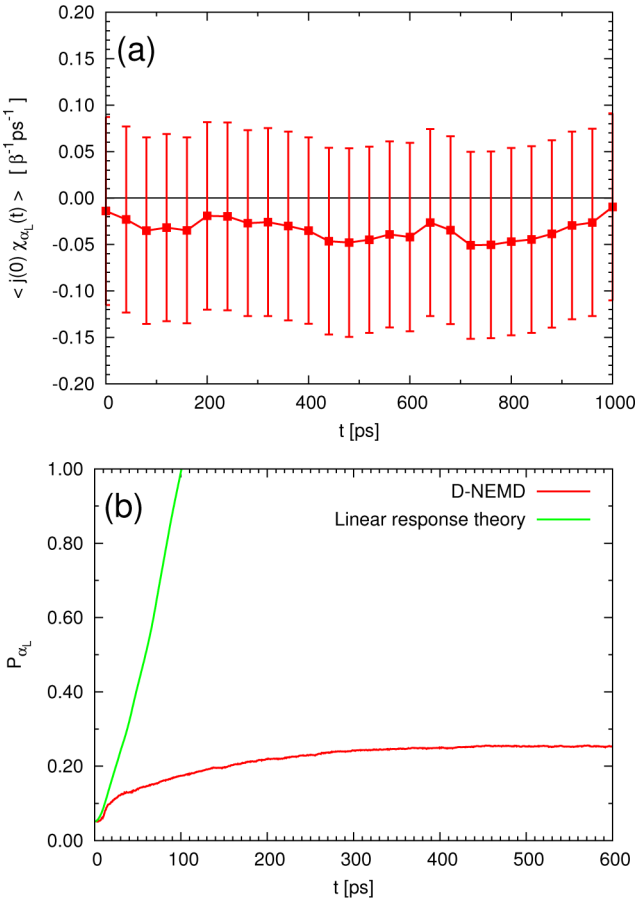

Figure 12. Numerical result of the linear response theory. (a) The correlation function $\langle j(0)\cdot\chi_{\alpha_L}(t)\rangle_0$ against time t. The error bars in the figure denote the statistical uncertainty at 95% confidence level. (b) The probability of conformation α_L computed from the linear response theory (12) versus that computed from D-NEMD (1).

AUTHOR INFORMATION

Corresponding Author

*E-mail: han.wang@fu-berlin.de.

Notes

The authors declare no competing financial interest.

ACKNOWLEDGMENTS

H.W. acknowledges the valuable discussions with Simone Meloni and Burkhard Schmidt. This work was partially supported by the Deutsche Forschungsgemeinschaft (DFG), with the Heisenberg Grant provided to L.D.S. (Grant No. DE 1140/5-1), and with the support within the priority program "Ionic Liquids" SPP 1191 (H.W. and L.D.S.). H.W. and C.S. thank the financial support by DFG research center MATHEON. Funding from the IIT SEED project SIMBEDD and from the SFI Grant 08-IN.1-I1869 is acknowledged by G.C.

REFERENCES

(1) Bohr, H.; Bohr, J. *Phys. Rev. E* **2000**, *61*, 4310.
(2) Bohr, H.; Bohr, J. *Bioelectromagnetics* **2000**, *21*, 68−72.
(3) de Pomerai, D.; Daniells, C.; David, H.; Allan, J.; Duce, I.; Mutwakil, M.; Thomas, D.; Sewell, P.; Tattersall, J.; Jones, D.; Candido, P. *Nature* **2000**, *405*, 417−418.
(4) Inskip, P. D.; Tarone, R. E.; Hatch, E. E.; Wilcosky, T. C.; Shapiro, W. R.; Selker, R. G.; Fine, H. A.; Black, P. M.; Loeffler, J. S.; Linet, M. S. *N. Engl. J. Med.* **2001**, *344*, 79−86.
(5) Mancinelli, F.; Caraglia, M.; Abbruzzese, A.; d'Ambrosio, G.; Massa, R.; Bismuto, E. *J. Cell. Biochem.* **2004**, *93*, 188−196.
(6) Budi, A.; Legge, F.; Treutlein, H.; Yarovsky, I. *J. Phys. Chem. B* **2005**, *109*, 22641−22648.
(7) Budi, A.; Legge, F.; Treutlein, H.; Yarovsky, I. *J. Phys. Chem. B* **2007**, *111*, 5748−5756.
(8) Budi, A.; Legge, F. S.; Treutlein, H.; Yarovsky, I. *J. Phys. Chem. B* **2008**, *112*, 7916−7924.
(9) Toschi, F.; Lugli, F.; Biscarini, F.; Zerbetto, F. *J. Phys. Chem. B* **2008**, *113*, 369−376.
(10) Astrakas, L.; Gousias, C.; Tzaphlidou, M. *J. Appl. Phys.* **2011**, *109*, 094702−094702.
(11) Astrakas, L. G.; Gousias, C.; Tzaphlidou, M. *J. Appl. Phys.* **2012**, *111*, 074702−074702.
(12) Damm, M.; Nusshold, C.; Cantillo, D.; Rechberger, G. N.; Gruber, K.; Sattler, W.; Kappe, C. O. *J. Proteomics* **2012**, *75*, 5533−5543.
(13) Starzyk, A.; Cieplak, M. *J. Chem. Phys.* **2013**, *139*, 045102.
(14) English, N.; Solomentsev, G.; O'Brien, P. *J. Chem. Phys.* **2009**, *131*, 035106.
(15) Solomentsev, G.; English, N.; Mooney, D. *J. Comput. Chem.* **2012**, *33*, 917−923.
(16) Ciccotti, G.; Jacucci, G. *Phys. Rev. Lett.* **1975**, *35*, 789.
(17) Ciccotti, G.; Jacucci, G.; McDonald, I. *J. Stat. Phys.* **1979**, *21*, 1−22.
(18) Ciccotti, G.; Pierleoni, C.; Ryckaert, J. Theoretical foundation and rheological applications of nonequilibrium molecular dynamics. In *Microscopic Simulations of Complex Hydrodynamic Phenomena*; Plenum Press: New York, 1993; pp 25−45.
(19) Palla, P.; Pierleoni, C.; Ciccotti, G. *Phys. Rev. E* **2008**, *78*, 021204.
(20) Orlandini, S.; Meloni, S.; Ciccotti, G. *Phys. Chem. Chem. Phys.* **2011**, *13*, 13177−13181.
(21) Orlandini, S.; Meloni, S.; Ciccotti, G. Hydrodynamics from dynamical NEMD. *AIP Conference Proceedings*; AIP Publishing LLC: Melville, NY, 2011; p 77.
(22) de la Hoz, A.; Diaz-Ortiz, A.; Moreno, A. *Chem. Soc. Rev.* **2005**, *34*, 164−178.
(23) Brooks, C., III; Karplus, M. *J. Chem. Phys.* **1983**, *79*, 6312.
(24) Foloppe, N.; MacKerell, A. D., Jr. *J. Comput. Chem.* **2000**, *21*, 86−104.
(25) Jorgensen, W. L.; Chandrasekhar, J.; Madura, J. D.; Impey, R. W.; Klein, M. L. *J. Chem. Phys.* **1983**, *79*, 926−935.
(26) MacKerell, A. D.; Feig, M.; Brooks, C. L., III *J. Comput. Chem.* **2004**, *25*, 1400−1415.
(27) Pronk, S.; Páll, S.; Schulz, R.; Larsson, P.; Bjelkmar, P.; Apostolov, R.; Shirts, M.; Smith, J.; Kasson, P.; van der Spoel, D.; E., H. B. L. *Bioinformatics* **2013**, 1−10.
(28) Bjelkmar, P.; Larsson, P.; Cuendet, M. A.; Hess, B.; Lindahl, E. *J. Chem. Theory Comput.* **2010**, *6*, 459−466.
(29) Darden, T.; York, D.; Pedersen, L. *J. Chem. Phys.* **1993**, *98*, 10089.
(30) Essmann, U.; Perera, L.; Berkowitz, M.; Darden, T.; Lee, H.; Pedersen, L. *J. Chem. Phys.* **1995**, *103*, 8577.
(31) Hess, B.; Bekker, H.; Berendsen, H.; Fraaije, J. *J. Comput. Chem.* **1997**, *18*, 1463−1472.
(32) Miyamoto, S.; Kollman, P. *J. Comput. Chem.* **2004**, *13*, 952−962.
(33) Parrinello, M.; Rahman, A. *J. Appl. Phys.* **1981**, *52*, 7182.
(34) Schütte, C.; Noé, F.; Lu, J.; Sarich, M.; Vanden-Eijnden, E. *J. Chem. Phys.* **2011**, *134*, 204105.
(35) Apostolakis, J.; Ferrara, P.; Caflisch, A. *J. Chem. Phys.* **1999**, *110*, 2099−2108.
(36) Gfeller, D.; De Los Rios, P.; Caflisch, A.; Rao, F. *Proc. Natl. Acad. Sci. U.S.A.* **2007**, *104*, 1817−1822.
(37) Scovell, D. L.; Pinkerton, T. D.; Medvedev, V. K.; Stuve, E. M. *Surf. Sci.* **2000**, *457*, 365−376.

(38) Vogel, A.; Linz, N.; Freidank, S.; Paltauf, G. *Phys. Rev. Lett.* **2008**, *100*, 38102.
(39) Plusquellic, D. F.; Siegrist, K.; Heilweil, E. J.; Esenturk, O. *ChemPhysChem* **2007**, *8*, 2412−2431.
(40) Born, B.; Kim, S. J.; Ebbinghaus, S.; Gruebele, M.; Havenith, M. *Faraday Discuss.* **2009**, *141*, 161−173.
(41) Vitalini, F.; Mey, A.; Noé, F.; Keller, B. *unpublished* 2013.
(42) Green, M. S. *J. Chem. Phys.* **1954**, *22*, 398−413.
(43) Kubo, R. *J. Phys. Soc. Jpn.* **1957**, *12*, 570−586.
(44) Tuckerman, M. *Statistical Mechanics: Theory and Molecular Simulation*; Oxford University Press: New York, 2010; p 499.